Scripta Materialia 142 (2018) 41–45

Contents lists available at ScienceDirect

Scripta Materialia

journal homepage: www.elsevier.com/locate/scriptamat

Regular article

Precipitation of α′ in neutron irradiated commercial FeCrAl alloys☆

Kevin G. Field [a,*], Kenneth C. Littrell [a], Samuel A. Briggs [b]

[a] Oak Ridge National Laboratory, Oak Ridge, TN 37831, USA
[b] University of Wisconsin, Madison, WI 53706, USA

ARTICLE INFO

Article history:
Received 27 March 2017
Received in revised form 3 July 2017
Accepted 14 August 2017
Available online xxxx

Keywords:
FeCrAl
Neutron diffraction
Precipitation
Ferritic steels

ABSTRACT

Alkrothal 720 and Kanthal APMT™, two commercial FeCrAl alloys, were neutron irradiated up to damage doses of 7.0 displacements per atom (dpa) in the temperature range of 320 to 382 °C to characterize the α′ precipitation in these alloys using small-angle neutron scattering. Both alloys exhibited α′ precipitation. Kanthal APMT™ exhibited higher number densities and volume fraction, a result attributed to its higher Cr content compared with Alkrothal 720. Trends observed as a function of damage dose (dpa) are consistent with literature trends for both FeCr and FeCrAl alloys.

High chromium (Cr) ferritic/martensitic steels are frequently investigated for applications requiring elevated temperatures and oxidation and/or corrosion resistance. The elevated Cr content (typically >7–8 at.%) enables acceptable oxidation and corrosion resistance in a range of elevated-temperature environments such as air, water, and steam. Many of these ferritic steel alloys are susceptible to embrittlement at service temperatures of ~500 °C or below. This embrittlement phenomenon is classically referred to as "475 °C embrittlement," and decades of research have been dedicated to understanding its cause. It is now accepted that the embrittlement results from a miscibility gap below 500 °C in the Fe-Cr phase diagram, where precipitation of the Cr-rich α′ phase occurs through either a nucleation and growth process or spinodal decomposition in the Fe-rich α matrix when the Cr content of the alloy exceeds ~8.5 at.% [1,2].

Detailed studies of the Fe-Cr system show that the mechanism, rate, and magnitude of the precipitation of the α′ phase depend on both the service temperature and composition of the ferritic-based stainless steel [3]. For example, Grobner [4] and Courtnall and Pickering [5] summarize the effects of alloying and show most practical alloying elements, such as Ti, Mo, and Nb, lead to an increased rate in hardening linked to α′ precipitation. Additional studies [2,6] show the detrimental effect of increased Cr content in FeCr alloys upon α′ precipitation and the resulting mechanical performance. It appears that traditional metallurgy practices have little effect on mitigating α′ embrittlement. However, renewed interest in FeCrAl-based alloys for applications below ~500 °C has triggered the rediscovery of the benefits of significant additions of aluminum (Al) (≥2.5 at.%) [7,8] on α′ precipitation. Although Al additions often provide a benefit in suppressing α′ precipitation, many industrial alloys—such as PM2000, MA956, and AISI Type 406—have proved to still be susceptible to α′ formation [9–14].

This study seeks to expand the current database of α′ precipitation in commercially available FeCrAl alloys to provide insight into their viability in industrial applications in which service temperatures reside below 500 °C. Specifically, the interest of this study is to examine candidate FeCrAl alloys for accident tolerant fuel (ATF) cladding applications where service temperatures are expected to be near 300 °C but off-normal conditions can exceed temperatures above 1000 °C [15]. Coupons of commercial alloys were neutron irradiated and then characterized using small-angle neutron scattering (SANS). Neutron irradiation has been shown to increase the rate of α′ precipitation [2,6,16–18] and hence accelerate the speed of detection of α′ and rapid progression to the growth-based regime for alloys where nucleation and growth is expected. SANS is widely used for characterization of α′ precipitation in both FeCr [13,18–21] and FeCrAl alloys [3,17,22,23], and our recent work shows good agreement can be achieved between SANS and more time-intensive atom probe tomography studies [17].

Two commercial FeCrAl alloys, Kanthal APMT™ and Alkrothal 720, were used for this study. Kanthal APMT™ is a 21.95 at.% Cr–9.64 at.% Al–1.52 at.% Mo, powder-metallurgy–derived FeCrAl alloy; the heat and hence composition is the same as in Ref. [24]. Alkrothal 720 is a 13.13 at.% Cr–8.22 at.% Al, wrought FeCrAl alloy; its composition and

* Corresponding author at: Materials Science and Technology Division, PO Box 2008, Oak Ridge, TN 37831, USA.
E-mail addresses: fieldkg@ornl.gov (K.G. Field), littrellkc@ornl.gov (K.C. Littrell), sbriggs@sandia.gov (S.A. Briggs).

http://dx.doi.org/10.1016/j.scriptamat.2017.08.022
1359-6462/

starting microstructure are found in Ref. [25]. Only two commercial alloys were studied due to the limited sample volume capacity of the neutron irradiation rig used. The selected alloys represent two uniquely different alloy types: one in which α′ precipitation is expected to occur in great magnitude (Kanthal APMT™) and one in which little or no α′ precipitation is expected (Alkrothal 720) but both alloys still exhibit high temperature (1200 °C) steam oxidation resistance, a key requirement for ATF cladding applications [26,27]. Additionally, the Mo additions in the Kanthal APMT™ alloy allow for possible insights into any additional effects due to minor alloying additions or powder metallurgy fabrication approach. Bulk Kanthal APMT™ was fabricated in rod form and bulk Alkrothal 720 specimens in thin sheet form.

Neutron irradiations were conducted in Oak Ridge National Laboratory's (ORNL's) High Flux Isotope Reactor (HFIR). Full details regarding the specimen configuration and irradiations are found in Refs. [16,17,23–25]; only a brief description is provided here. Kanthal APMT™ was neutron irradiated to 0.3, 1.8, and 7.0 displacement per atom (dpa) at temperatures of 334.5 ± 0.6 °C, 381.9 ± 5.4 °C, and 319.9 ± 12.7 °C, respectively. Alkrothal 720 was neutron irradiated to 0.8, 1.8, and 7.0 dpa at temperatures of 355.1 ± 3.4 °C, 381.9 ± 5.4 °C, and 319.9 ± 12.7 °C, respectively. The dose ranges represent the transient regime for the mechanical properties of FeCrAl alloys under irradiation conditions relevant toward early- to mid-life cladding conditions during light water reactor operation [24]. All irradiations were conducted with a neutron flux between 8.54×10^{14} and 8.84×10^{14} n/cm^2 s (E > 0.1 MeV), resulting in dose rates in the range of 7.7×10^{-7} to 8.1×10^{-7} dpa/s.

Tensile coupons of both the as-received and neutron-irradiated condition were tested in a shielded hot cell facility; data from these tests are presented elsewhere [24,28]. Following the tensile tests, one-half of each broken tensile specimen was prepared and shipped to the HFIR General Purpose SANS [29] beam line. The SANS detector configuration and data reduction techniques were identical to those described in Ref. [17].

Scattering intensities were modeled using a simplified approach in which α′ precipitates are considered monodispersed spheres within the α matrix and exhibit a hard-sphere potential. Additionally, an inherent background contribution was found owing to large impurities, precipitates, and grain boundaries in the alloys that result in an additional low-q inverse power law completed in summation [30]. No contribution of the reactive element-rich particles in the Kanthal APMT™ specimens in the q-range studied were observed due to their large particles sizes (100–500 nm) [31]. The result is that $I(q)$ takes the functional form of

$$I(q) = V\eta^{\alpha'}\Delta\rho^2 P(q,r)S(q,R_{hs},\eta) + (Aq^{-m} + B), \quad (1)$$

where V is the volume of the precipitates; $\eta^{\alpha'}$ is the volume fraction of α′ precipitates; $\Delta\rho$ is the scattering length density difference between the α′ phase and the α matrix; $P(q,r)$ is the particle form factor for spherical precipitates [32]; $S(q,R_{hs},\eta)$ is the hard-sphere structure factor [30]; and $Aq^{-m} + B$ is the inverse power law, where A is the power law length scale factor, m is the power law exponent, and B is the residual background in the measurements. This functional form was fitted to the experimental data using a modified Levenberg-Marquardt algorithm. Values of interest, including precipitate volume fraction, number density, and radius of the α′ precipitates, can be derived from the fitting parameters using the method described by Pedersen [30]. Using simplifying assumptions in the determined scattering contrast, as described in previous work [17], the composition of the α′ precipitates and the α matrix can be estimated by

$$C_{Cr}^{matrix} = \overline{C}_{Cr} - \frac{\eta^{\alpha'}\Delta\rho a_o^3}{4(b_{Fe} - b_{Cr})} \quad (2)$$

and

$$C_{Cr}^{\alpha'} = \left[\overline{C}_{Cr} - \left(1 - \eta^{\alpha'}\right)C_{Cr}^{matrix}\right]/\eta^{\alpha'}, \quad (3)$$

where $\overline{C}_{Cr}$ is the bulk composition of Cr in atomic fraction, C_{Cr}^{matrix} is the atomic fraction of Cr in the matrix, $C_{Cr}^{\alpha'}$ is the atomic fraction of Cr in the α′ precipitates, a_o is the lattice parameter (2.87 Å), and b_{Fe} and b_{Cr} are scattering lengths of Fe and Cr respectively. Reported errors for all values are based on the standard error of the fitting coefficients and any subsequent error propagation [30]. The assumed model has been applied to neutron-irradiated model FeCrAl alloys and shown good experimental matching for both morphology and composition values with atom probe tomography results at higher doses where a coarsening regime is expected [17].

Fig. 1 shows the scattering curves, including the best-fit determined model for both alloys. The unirradiated curves in Fig. 1 show only the low-Q inverse power law contribution to the scattering curves, indicating no significant Cr-clustering or α′ precipitation in these alloys before irradiation. After irradiation, a characteristic peak is observed in the SANS scattering curves stemming from the presence of α′ precipitates within the matrix. A clear change in this peak with increasing damage dose (dpa) is seen for both Kanthal APMT™ and Alkrothal 720. For both alloys, the peaks shift toward lower Q and the magnitude of the peaks increase with increasing damage dose (dpa). The relative change in this trend is more apparent in higher-Cr Kanthal APMT™ than in Alkrothal 720. Qualitatively, these trends suggest that with increasing dose, a lower number density of precipitates are present in both alloys; but a significantly higher volume fraction exists within the Kanthal APMT™ matrix, as expected.

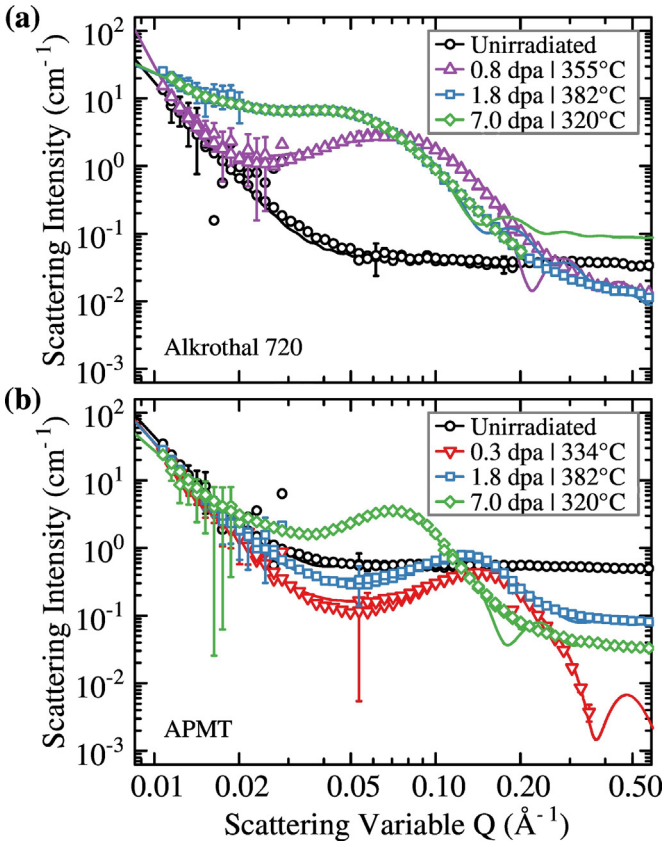

Fig. 1. Experimental scattering intensities (symbols) and best-fit model (lines) of neutron-irradiated commercial FeCrAl alloys: (a) Alkrothal 720 and (b) Kanthal APMT™.

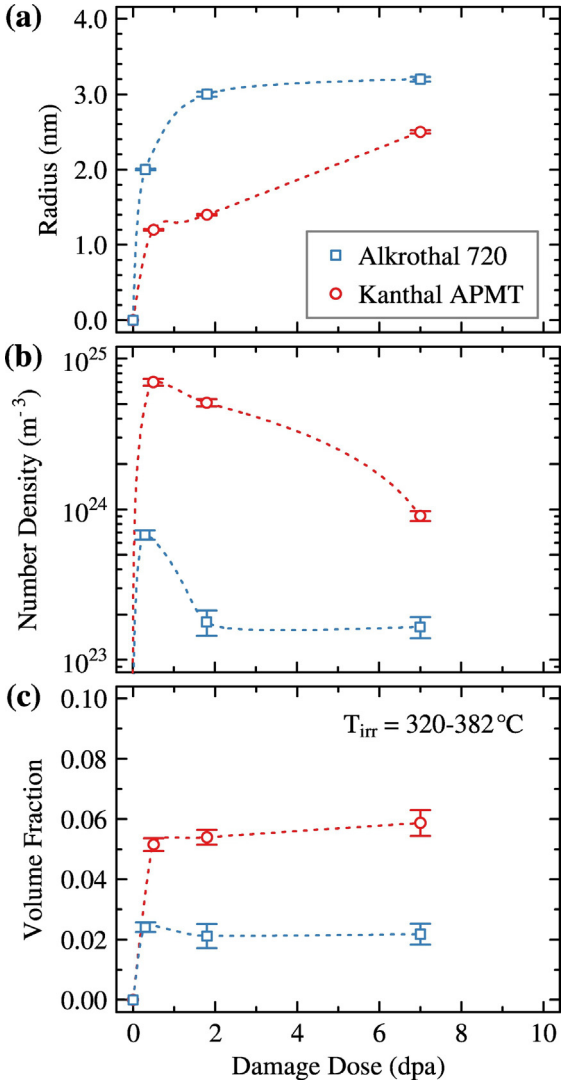

Fig. 2. Alkrothal 720 and Kanthal APMT™ (a) change in radius, (b) number density, and (c) volume fraction for α′ precipitation after neutron irradiation up to 7.0 dpa at temperatures of 320 to 382 °C (T_{irr}). Dotted lines are fitted splines.

Fig. 2 shows the quantitative change in the size, number density, and volume fraction of the α′ precipitates as a function of damage dose for both alloys. An increase in the precipitate sizes is observed for both alloys with increasing dose, although it appears that Alkrothal 720 approaches saturation near 1.8 dpa. Kanthal APMT™ does not reach saturation within the same dose regime, as indicated by the rapid increase in size between the 1.8 dpa and 7.0 dpa conditions. Note that the 1.8 dpa condition had the highest irradiation temperature (382 °C); hence, deviations from a natural trend are expected. Across the whole dose range investigated, Alkrothal 720 consistently showed larger α′ precipitate sizes than Kanthal APMT™.

The number density of precipitates decreases with increasing damage dose above 0.3 dpa (Fig. 2b). For Kanthal APMT™, a near order of magnitude difference is observed between the lowest-dose condition and the 7.0 dpa condition. Again, it appears that Alkrothal 720 reaches saturation at 1.8 dpa, as no change within the error of the measurement is observed at and above this dose. Alkrothal 720 had the lowest number density across all doses investigated. Contrary to the size and number density trends, the volume fraction remained unchanged with increasing damage dose when statistical error in the model was considered. However, the volume fraction observations and number density observations were consistent in the two alloys, with Alkrothal 720 having the lowest fraction of α′ precipitates in the ferrite matrix (Fig. 2c). The nearly constant volume fraction for a given alloy suggests a Lifshitz and Slyozov [33] and Wagner [34] (LSW)-type theory, which is based on Ostwald ripening (particle coarsening) mechanisms. Given this, the limited number of data points in a short dose (and time at temperature) range inhibits explicitly determining the adherence of the studied systems to this theory.

The observed trends were consistent with previous studies of both aged and neutron-irradiated FeCr and FeCrAl alloys. For example, Messoloras et al. and Cook et al. show that as aging time increases the number density steadily decreases, while the mean radius increases but the rate of change follows a diminishing return trend [3,35]. Furthermore, the effect of composition is consistent with our previous studies of neutron irradiated model FeCrAl alloys. Higher–Cr content FeCrAl alloys consistently show higher number densities and volume fractions than lower–Cr content FeCrAl alloys [16,17,23]. Here, there is a difference of 8.82 at.% Cr between the composition of Kanthal APMT ™ and Alkrothal 720, but only a 1.42 at.% variation in Al. The large variation in bulk-matrix pre-irradiation Cr content and nearly one order of magnitude difference in the number density of α′ in each dose range between the two alloys highlights the critical role of Cr content in α′ precipitation in commercial FeCrAl alloys, and reinforces its role in model FeCrAl alloys.

Kanthal APMT™ also contains 1.52 at.% Mo. Courtnall and Pickering [5] indicated increased hardening linked to α′ precipitation via either a Cr-Mo complex formation leading to enhanced nucleation or that Mo increases the coherency strains of α′ resulting in increased age hardening for model FeCr alloys. Here, neither effect can be supported or refuted as the large variation in the bulk-matrix pre- irradiation Cr content overshadows any minor alloy effects. A systematic study where the Mo content is varied while the Cr content remains constant is needed to further define the mechanisms contributing to the observed processes by Courtnall and Pickering, but fell out of the current scope of this study.

Limited studies have been completed on the Cr-content within α′ precipitates in the FeCrAl system. PM2000 is the only commercial FeCrAl alloy exhaustively studied for the composition of α′; it has been shown that, with sufficient aging time and temperature (≥1000 h at 475 °C), the Cr content in α′ reaches ~80–85 at.%, which are typical values reported for α′ in the FeCr system (see Ref. [11] and additional studies by these authors). The time to reach these composition values was delayed with reduced aging temperature in PM2000; e.g., at 1000 h at 400 °C, the Cr content was only 28.9 at.%. In neutron-irradiated Kanthal APMT™ and Alkrothal 720, the Cr content of the α′ precipitates was estimated not to reach the final saturation value shown by Capdevila et al. (Fig. 3b). For both alloys, the Cr content mean value was 66 at.% Cr (Fig. 3b). The observed trend, compared with previous results for PM2000, suggests the saturation values have not been met, but the rate toward these values has increased. Such an effect is consistent with the expected precipitation enhancement in irradiated samples versus thermally aged samples due to a radiation-enhanced diffusion mechanism. Because of the lower-temperature irradiation (320–382 °C), relatively low maximum dose/time at temperature (7.0 dpa, 2456 h at 320 °C), and large error due to the simplifying assumptions used to derive Eqs. (2) and (3), the saturation values for α′ cannot be experimentally determined in this study.

Kobayashi and Takasugi [8] provided a α–α′ boundary for the FeCrAl system using diffusion multiples at 475 °C, but they investigated only one temperature and used an arbitrary cut-off for change in hardness values in which the α–α′ boundary was derived from. The FeCr and Fe-Cr-8.0Al at.% alloys phase diagrams in Wukusick [7] and the more recent FeCr phase diagram in Bonny et al. [2] show that at lower temperatures than 475 °C that lower Cr-content (~1.5–2 at.% lower) reside within the α + α′ region of the phase diagrams. This temperature effect in the Fe-rich corner of the Fe-Cr-Al phase diagram was recently highlighted by Ejenstam et al. using a kinetic Monte Carlo model and

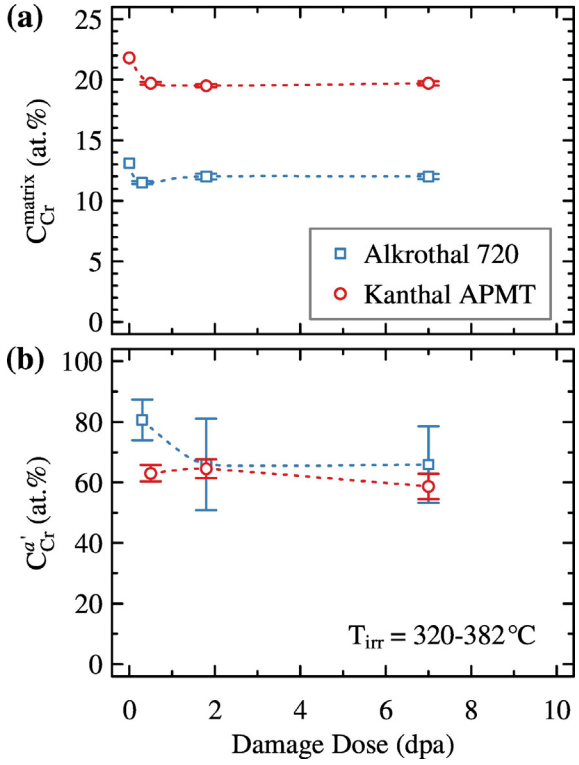

Fig. 3. Change in matrix Cr content (a) and α′ Cr content (b) up to 7.0 dpa at temperatures of 320 to 382 °C (T_{irr}) in Alkrothal 720 and Kanthal APMT™. Dotted lines are fitted splines.

showed a decrease from 475 °C to 338 °C results in the phase boundary shifting toward lower-Cr for a given Al content [36].

Fig. 4 shows the iron-rich corner of the Fe-Cr-Al system and plots the experimental results of this study, along with current literature of both commercial and model FeCrAl alloys. All experimental data below 500 °C where SANS or microscopy-based techniques were completed is presented; restricting to a single temperature (i.e. 475 °C) would lead to limited data points preventing determination of known compositions

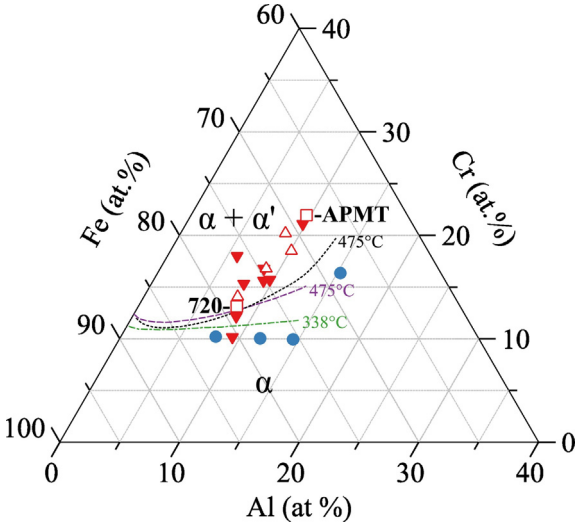

Fig. 4. FeCrAl alloy susceptibility to α′ below 500 °C. Red down-closed triangles are model FeCrAl alloys shown to form α′ [3,16,17,23,36–38], red up-open triangles are commercial FeCrAl alloys shown to form α′ [9–14], blue closed circles are model FeCrAl alloys not forming α′ [37,39], and red open-squares are from this study. Dotted black line is an experimentally determined α–α′ phase boundary at 475 °C [8] while the dotted green and purple line are computationally determined α–α′ phase boundaries at 338 °C and 475 °C, respectively [37]. (For interpretation of the references to color in this figure legend, the reader is referred to the web version of this article.)

with α′ susceptibilities. The α–α′ boundary at 475 °C proposed by Kobayashi and Takasugi [8] and at 475 °C and 338 °C by Ejenstam et al. [36] is reproduced in Fig. 4 to provide insight into the role of temperature on α′ formation as a function of composition. This study supports the boundaries in Fig. 4. The trends observed between Kanthal APMT™ and Alkrothal 720 are consistent, as Alkrothal 720 resides near the proposed phase boundary and hence a lower volume fraction of α′ should exist than in Kanthal APMT™, which resides well within the α + α′ regime.

Note that in a previous study, Fe-10Cr-9.34Al in at.% was observed to form α′ after neutron irradiation, although another alloy with Fe-10Cr-7.9Al in at.% was found not to form α′ after thermal aging (Fig. 4). The variation could be due to temperature, as illustrated by Wukusick and Ejenstam, as the FeCrAl alloy with 9.34 at.% Al was studied at temperatures between 320 and 383 °C [17,23], whereas the other alloy was studied at temperatures of 450, 500, and 550 °C [36]. The difference between irradiation studies and thermal aging studies can also not be ruled out. Irradiation leads to the formation of point defects which can increase the diffusion as well as agglomerate creating extended defects which could act as preferential nucleation sites for precipitates. Recent characterization has shown that extended radiation-induced defects are not co-located spatially with α′ precipitates in FeCrAl alloys [37], indicating that α′-formation is most likely enhanced under irradiation due to radiation-enhanced diffusion. Thus, it could also be proposed that α′ precipitation could occur within the Fe-10Cr-7.9Al alloy, but it was not observed due to the sluggish kinetics under the thermal aging conditions of that study.

In summary, two commercial FeCrAl alloys, Alkrothal 720 and Kanthal APMT™, were neutron irradiated and then characterized for α′ precipitation using SANS. Observed trends in size, number density, and volume fraction were consistent with the growing database on α′ formation in FeCr and FeCrAl alloys. The large variation in Cr content (8.82 at.%) between the alloys caused the higher-Cr variation, Kanthal APMT™, to have a higher volume fraction and number density for any studied irradiation condition. This result specifically highlights the role of Cr composition in α′ precipitation in both model and commercial FeCrAl alloys.

Acknowledgments

The authors thank ORNL's Thermal Hydraulics and Irradiation Engineering Group, Irradiated Materials Examination and Testing facility, and Low Activation Materials Development and Analysis facility staff for their continuing support of this research. Additionally, the authors would like to thank R.H. Howard of ORNL for his thoughtful design and implementation of the irradiation capsules within HFIR.

Research was sponsored by the Department of Energy (DOE) Office of Nuclear Energy, Advanced Fuel Campaign of the Fuel Cycle R&D program. ORNL's HFIR is sponsored by the DOE Office of Science, Basic Energy Sciences (BES), and use of the General-Purpose SANS beamline at HFIR's user facility was sponsored by DOE-BES Scientific User Facilities Division. A portion of support for one author (SAB) was provided by the DOE Office of Nuclear Energy University Programs.

References

[1] R.O. Williams, Trans. Metall. Soc. AIME 212 (1958) 497–502.
[2] G. Bonny, D. Terentyev, L. Malerba, Scr. Mater. 59 (2008) 1193–1196, http://dx.doi.org/10.1016/j.scriptamat.2008.08.008.
[3] J. Cook, A.C. Roberts, C.G. Windsor, B.C. Pike, R.J. Stewart, CookPaper.pdf, Adv. Phys. Metall. Appl. Steels, The Metals Society, 1981 362–368.
[4] P.J. Grobner, Metall. Trans. A. 4 (1973) 251–260.
[5] M. Courtnall, F.B. Pickering, Met. Sci. 10 (1976) 273–276, http://dx.doi.org/10.1179/030634576790432353.
[6] M. Bachhav, G. Robert Odette, E.A. Marquis, Scr. Mater. 74 (2014) 48–51, http://dx.doi.org/10.1016/j.scriptamat.2013.10.001.
[7] C.S. Wukusick, The Physical Metallurgy and Oxidation Behavior of Fe-Cr-Al-Y Alloys, Cincinnati, Ohio, 1966.

[8] S. Kobayashi, T. Takasugi, Scr. Mater. 63 (2010) 1104–1107, http://dx.doi.org/10.1016/j.scriptamat.2010.08.015.
[9] H.G. Read, H. Murakami, Appl. Surf. Sci. 94 (1996) 334–342.
[10] H.G. Read, H. Murakami, K. Hono, Scr. Mater. 36 (1997) 355–361.
[11] C. Capdevila, M.K. Miller, J. Chao, Acta Mater. 60 (2012) 4673–4684, http://dx.doi.org/10.1016/j.actamat.2012.05.022.
[12] M. Pinkas, Z. Foxman, N. Froumin, P. Hähner, L. Meshi, J. Mater. Sci. 50 (2015) 4629–4635, http://dx.doi.org/10.1007/s10853-015-9014-0.
[13] Z. Száraz, G. Török, V. Kršjak, P. Hähner, J. Nucl. Mater. 435 (2013) 56–62, http://dx.doi.org/10.1016/j.jnucmat.2012.12.016.
[14] G. Electric, ^{630}A Mark V Maritime Nuclear Steam Generator Design Studies Summary, GEMP-359, 1965.
[15] K.A. Terrani, S.J. Zinkle, L.L. Snead, J. Nucl. Mater. 448 (2013) 420–435, http://dx.doi.org/10.1016/j.jnucmat.2013.06.041.
[16] P.D. Edmondson, S.A. Briggs, Y. Yamamoto, R.H. Howard, K. Sridharan, K.A. Terrani, et al., Scr. Mater. 116 (2016) 112–116, http://dx.doi.org/10.1016/j.scriptamat.2016.02.002.
[17] S.A. Briggs, P.D. Edmondson, Y. Yamamoto, C. Littrell, R.H. Howard, C.R. Daily, et al., Acta Mater. 129 (2016) 217–228.
[18] M.H. Mathon, Y. de Carlan, G. Geoffroy, X. Averty, A. Alamo, C.H. de Novion, J. Nucl. Mater. 312 (2003) 236–248, http://dx.doi.org/10.1016/s0022-3115(02)01630-6.
[19] M.-H. Mathon, Y. De Carlan, X. Averty, A. Alamo, C.-H. De Novion, Small angle neutron scattering study of irradiated martensitic steels: relation between microstructural evolution and hardening, J. ASTM Int. 2 (2005). www.astm.org (accessed August 26 2016).
[20] C. Heintze, F. Bergner, A. Ulbricht, H. Eckerlebe, J. Nucl. Mater. 409 (2011) 106–111, http://dx.doi.org/10.1016/j.jnucmat.2010.09.010.
[21] A. Ulbricht, C. Heintze, F. Bergner, H. Eckerlebe, J. Nucl. Mater. 407 (2010) 29–33, http://dx.doi.org/10.1016/j.jnucmat.2010.07.005.
[22] S. Messoloras, B.C. Pike, R.J. Stewart, C.G. Windsor, Met. Sci. 18 (1984) 311–321.
[23] K.G. Field, X. Hu, K.C. Littrell, Y. Yamamoto, L.L. Snead, J. Nucl. Mater. 465 (2015) 746–755, http://dx.doi.org/10.1016/j.jnucmat.2015.06.023.
[24] K.G. Field, S.A. Briggs, K. Sridharan, R.H. Howard, Y. Yamamoto, J. Nucl. Mater. 489 (2017) 118–128.
[25] K.G. Field, S.A. Briggs, X. Hu, Y. Yamamoto, R.H. Howard, K. Sridharan, J. Nucl. Mater. 483 (2017) 54–61, http://dx.doi.org/10.1016/j.jnucmat.2016.10.050.
[26] B.A. Pint, K.A. Unocic, K.A. Terrani, Mater. High Temp. 32 (2014) 28–35.
[27] K.A. Unocic, Y. Yamamoto, B.A. Pint, Oxid. Met. 87 (2017) 431–441, http://dx.doi.org/10.1007/s11085-017-9745-1.
[28] K.G. Field, S.A. Briggs, P.D. Edmondson, J.C. Haley, R.H. Howard, X. Hu, et al., Database on Performance of Neutron Irradiated FeCrAl Alloys, ORNL/TM-2016/335, 2016.
[29] G.D. Wignall, K.C. Littrell, W.T. Heller, Y.B. Melnichenko, K.M. Bailey, G.W. Lynn, et al., J. Appl. Crystallogr. 45 (2012) 990–998, http://dx.doi.org/10.1107/s0021889812027057.
[30] J. Skov Pedersen, Phys. Rev. B 47 (1993).
[31] J. Engkvist, A.S. Canovic, A.K. Hellström, A.A. Järdnäs, J.-E. Svensson, A.L.-G. Johansson, et al., Oxid. Met. 73 (2010) 233–253, http://dx.doi.org/10.1007/s11085-009-9177-7.
[32] L. Rayleigh, Proc. R. Soc. Lond. A 84 (1910) 25–46, http://dx.doi.org/10.1098/rspa.1910.0054 (Published 9 June 1910).
[33] I.M. Lifshitz, V.V. Slyozov, J. Phys. Chem. Solids 1 (19) (1961) 35–50.
[34] C. Wagner, Zeitschrift Für Elektrochemie 65 (1961) 581.
[35] S. Messoloras, B.C. Pike, R.J. Stewart, C.G. Windsor, Met. Sci. 18 (1984).
[36] J. Ejenstam, M. Thuvander, P. Olsson, F. Rave, P. Szakalos, J. Nucl. Mater. (2014)http://dx.doi.org/10.1016/j.jnucmat.2014.11.101.
[37] S.A. Briggs, K. Sridharan, K.G. Field, Adv. Mater. Process. 174 (2016) 16–21.
[38] W. Han, K. Yabuuchi, A. Kimura, S. Ukai, N. Oono, T. Kaito, et al., Nucl. Mater. Energy. 9 (2016) 610–615, http://dx.doi.org/10.1016/j.nme.2016.05.015.